A Surprisingly Large Thermal Hysteresis Loop in a Reversible Phase Transition of $Rb_xMn[Fe(CN)_6]_{(x+2)/3}\cdot zH_2O$

Shin-ichi Ohkoshi,*,†,‡ Tomoyuki Matsuda,† Hiroko Tokoro,† and Kazuhito Hashimoto*,†

Department of Applied Chemistry, School of Engineering, The University of Tokyo, 7-3-1 Hongo, Bunkyo-ku, Tokyo 113-8656, Japan, and PRESTO, JST, 4-1-8 Honcho Kawaguchi, Saitama, Japan

Received September 8, 2004. Revised Manuscript Received October 13, 2004

A series of $Rb_xMn[Fe(CN)_6]_{(x+2)/3}\cdot zH_2O$ compounds ($x = 0.94$ (**1**), $x = 0.85$ (**2**), and $x = 0.73$ (**3**)) showed a temperature-induced phase transition with a thermal hysteresis loop, which is caused by the charge transfer from Mn^{II} to Fe^{III} and a Jahn−Teller distortion of the produced Mn^{III}. The transition temperature T_p and the width of a thermal hysteresis loop ΔT systematically changed with decreasing Fe/Mn ratio of $(x + 2)/3$; i.e., the T_p value decreased ($T_p = 259$ K (**1**), 236 K (**2**), and 205 K (**3**)) and the ΔT value increased ($\Delta T = 86$ K (**1**), 94 K (**2**), and 116 K (**3**)). It is noteworthy that a surprisingly large ΔT value of 116 K was recorded for **3**. The trends of the T_p shift and ΔT expansion were understood by the variation in the transition enthalpy based on the thermodynamical analysis. The crystal structures of the low-temperature (LT) phase for **1** and **2** were tetragonal structures, while the LT phase for **3** had a cubic structure. This difference is because the Jahn−Teller elongation of Mn^{III} is randomly oriented due to a low $Mn^{III}/(Mn^{II} + Mn^{III})$ ratio in the LT phase for **3**.

1. Introduction

Research associated with a thermal phase transition phenomenon is an attractive topic in the field of solid-state physics and chemistry.[1] A thermal phase transition is related to the cooperativity of the corresponding system and in a metal complex assembly is due to the interaction between a metal ion and lattice strain such as electron−phonon coupling,[2] Jahn−Teller distortions,[3] and elastic interactions.[4] When the cooperativity is strong, a thermal phase transition often accompanies a thermal hysteresis loop. Transition-metal complex assemblies,[5,6] such as cyano-bridged metal complex assemblies,[7−9] are condensed matters that have a strong cooperativity since the transition-metal ions are bridged by ligands with a 3-D network structure. Recently, we observed a temperature-induced phase transition, which is caused by a metal-to-metal charge transfer from Mn^{II} to Fe^{III} and a Jahn−Teller distortion of the produced Mn^{III} ion, with a thermal hysteresis loop in $RbMn[Fe(CN)_6]$.[10] In this phase transition, the high-temperature (HT) and low-temperature (LT) phases consist of $Fe^{III}(S = 1/2)$−CN−$Mn^{II}(S = 5/2)$ and $Fe^{II}(S = 0)$−CN−$Mn^{III}(S = 2)$ electronic states, respec-

* To whom correspondence should be addressed. E-mail: ohkoshi@light.t.u-tokyo.ac.jp (S.O.); hashimoto@light.t.u-tokyo.ac.jp (K.H.).

† The University of Tokyo.

‡ JST.

(1) (a) Gütlich, P. *Struct. Bonding (Berlin)* **1981**, *44*, 83. (b) Gütlich, P.; Hauser, A. *Coord. Chem. Rev.* **1990**, *97*, 1. (c) Kahn, O. *Molecular Magnetism*; VCH: New York, 1993. (d) Kahn, O.; Kröber, J.; Jay, C. *Adv. Mater.* **1992**, *4*, 718. (e) Kahn, O.; Martinez, J. C. *Science* **1998**, *279*, 44.

(2) Zimmermann, R. *J. Phys. Chem. Solids* **1983**, *44*, 151.

(3) (a) Kambara, T. *J. Phys. Soc. Jpn.* **1980**, *49*, 1806. (b) Sasaki, N.; Kambara, T. *J. Chem. Phys.* **1981**, *74*, 3472. (c) Kambara, T. *J. Chem. Phys.* **1981**, *74*, 4557.

(4) (a) Ohnishi, S.; Sugano, S. *J. Phys.* **1981**, *C14*, 39. (b) Spiering, H.; Meissner, E.; Köppen, H.; Müller, E. W.; Gütlich, P. *Chem. Phys.* **1982**, *68*, 65. (c) Boukheddaden, K.; Shteto, I.; Hôo, B.; Varret, F. *Phys. Rev. B* **2000**, *62*, 14796. (d) Boukheddaden, K.; Linares, J.; Codjovi, E.; Varret, F.; Niel, V.; Real, J. A. *J. Appl. Phys.* **2003**, *93*, 7103.

(5) (a) Desiraju, G. *Crystal Engineering: The Design of Organic Solids*; Elsevier Science Publishers B.V.: Amsterdam, The Netherlands, 1989. (b) Lehn, J. M. *Supramolecular Chemistry: Concepts and Perspectives*; VCH: Weinheim, Germany, 1995.

(6) (a) Li, H.; Eddaoudi, M.; O'Keeffe, M.; Yaghi, O. M. *Nature* **1999**, *402*, 276. (b) Kondo, M.; Asami, T.; Kitagawa, S.; Ishii, T.; Matsuzaka, H.; Seki, K. *Angew. Chem., Int. Ed.* **1999**, *38*, 140.

(7) (a) Verdaguer, M.; Bleuzen, A.; Marvaud, V.; Vaissermann, J.; Seuleiman, M.; Desplanches, C.; Scuiller, A.; Train, C.; Grade, R.; Gelly, G.; Lomenech, C.; Rosenman, I.; Veillet, P.; Cartier, C.; Villain, F. *Coord. Chem. Rev.* **1999**, *190*, 1023. (b) Ohkoshi, S.; Hashimoto, K. *J. Photochem. Phtotobiol., C* **2001**, *2*, 71. (c) Miller, J. S. *MRS Bull.* **2000**, *25*, 60.

(8) (a) Ludi, A.; Güdel, H. U. *Struct. Bonding (Berlin)* **1973**, *14*, 1. (b) Mallah, T.; Thiébaut, S.; Verdaguer, M.; Veillet, P. *Science* **1993**, *262*, 1554. (c) Verdaguer, M.; Mallah, T.; Gadet, V.; Castro, I.; Hélary, C.; Thiébaut, S.; Veillet, P. *Conf. Coord. Chem.* **1993**, *14*, 19. (d) Entley, W. R.; Girolami, G. S. *Science* **1995**, *268*, 397. (e) Ferlay, S.; Mallah, T.; Ouahès, R.; Veillet, P.; Verdaguer, M. *Nature* **1995**, *378*, 701. (f) Sato, O.; Iyoda, T.; Fujishima, A.; Hashimoto, K. *Science* **1996**, *271*, 49. (g) Buschmann, W. E.; Paulson, S. C.; Wynn, C. M.; Girtu, M. A.; Epstein, A. J.; White, H. S.; Miller, J. S. *Adv. Mater.* **1997**, *9*, 645. (h) Ohkoshi, S.; Hashimoto, K. *Chem. Phys. Lett.* **1999**, *314*, 210. (i) Ohkoshi, S.; Abe, Y.; Fujishima, A.; Hashimoto, K. *Phys. Rev. Lett.* **1999**, *82*, 1285. (j) Holmes, S. M.; Girolami, G. S. *J. Am. Chem. Soc.* **1999**, *121*, 5593. (k) Hatlevik, Ø.; Buschmann, W. E.; Zhang, J.; Manson, J. L.; Miller, J. S. *Adv. Mater.* **1999**, *11*, 914. (l) Ohkoshi, S.; Mizuno, M.; Hung, G. J.; Hashimoto, K. *J. Phys. Chem.* **2000**, *104*, 9365.

(9) (a) Garde, R.; Desplanches, C.; Bleuzen, A.; Veillet, P.; Verdaguer, M. *Mol. Cryst. Liq. Cryst.* **1999**, *334*, 587. (b) Ohkoshi, S.; Machida, N.; Zhong, Z. J.; Hashimoto, K. *Synth. Met.* **2001**, *122*, 523. (c) Rombaut, G.; Verelst, M.; Golhen, S.; Ouahab, L.; Mathoniere, C.; Kahn, O. *Inorg. Chem.* **2001**, *40*, 1151. (d) Zhong, Z. J.; Seino, H.; Mizobe, Y.; Hidai, M.; Fujishima, A.; Ohkoshi, S.; Hashimoto, K. *J. Am. Chem. Soc.* **2000**, *122*, 2952. (e) Larionova, J.; Gross, M.; Pilkington, M.; Andres, H.; Stoeckli, E. H.; Güdel, H. U.; Decurtins, S. *Angew. Chem., Int. Ed.* **2000**, *39*, 1605. (f) Podgajny, R.; Korzeniak, T.; Balanda, M.; Wasiutynski, T.; Errington, W.; Kemp, T. J.; Alcock, N. W.; Sieklucka, B. *Chem. Commun.* **2002**, *10*, 1138. (g) Li, D.; Gao, S.; Zheng, L.; Tang, W. *J. Chem. Soc., Dalton Trans.* **2002**, *14*. 2805. (h) Arimoto, Y.; Ohkoshi, S.; Zhong, Z. J.; Seino, H.; Mizobe, Y.; Hashimoto, K. *J. Am. Chem. Soc.* **2003**, *125*, 9240.

10.1021/cm048461x CCC: $30.25
Published on Web 12/13/2004

tively. A material that exhibits a large thermal hysteresis loop is useful for studying the cooperative interaction in condensed matter and an industrial application such as a memory device. In this work, we tried to expand the width of the thermal hysteresis loop of a rubidium−manganese hexacyanoferrate by tuning the composition. The prepared $Rb_xMn[Fe(CN)_6]_{(x+2)/3}\cdot zH_2O$ exhibited a temperature-induced phase transition with a surprisingly large thermal hysteresis loop that depends on x, i.e., 86 K ($x = 0.94$), 94 K ($x = 0.85$), and 116 K ($x = 0.73$). The observed thermal hysteresis of 116 K is the largest value observed for a reversible thermal hysteresis loop in an Fe-based compound. This expansion of the observed thermal hysteresis loop was discussed using a thermodynamical analysis.

2. Experimental Section

Target materials were prepared by reacting an aqueous solution of $MnCl_2$ (0.1 mol dm^{-3}) with a mixed aqueous solution of RbCl (0.2, 0.4, and 0.8 mol dm^{-3}) and $K_3[Fe(CN)_6]$ (0.1 mol dm^{-3}) to yield a precipitate: [RbCl] = 0.8 mol dm^{-3} (compound **1**), 0.4 mol dm^{-3} (compound **2**), and 0.2 mol dm^{-3} (compound **3**). The precipitates were filtered and dried, yielding powders.

Elemental analyses in the synthesized samples were performed using inductively coupled plasma mass spectrometry (ICP-MS) for Rb, Mn, and Fe elements and standard microanalytical methods for C and N elements. The water contents of the samples were determined by the least-squares approach of $\sum_i(w_{i,\text{found}} - w_{i,\text{calcd}})$,[2] where w_i is the weight percentage of Rb, Mn, Fe, C, and N elements in $Rb_xMn[Fe(CN)_6]_{(x+2)/3}\cdot zH_2O$. The morphology of the compounds was measured using scanning electron microscopy (SEM) (Hitachi S 4200) with a 3.5 kV accelerating voltage and a 30 μA beam current for imaging. Infrared (IR) spectra were recorded on a Shimadzu FT-IR 8200PC spectrometer. The XRD patterns (Cu Kα) were measured with a Rigaku RINT2100 instrument. During XRD measurement, the powder samples were placed on a Cu plate. Magnetic properties were investigated using a Quantum Design MPMS-7S superconducting quantum interference device (SQUID) magnetometer.

3. Results and Discussion

3.1. Materials. The precipitates were light brown powders. Elemental analyses for Rb, Mn, and Fe showed that the formulas of the obtained precipitates are $Rb_{0.94}Mn[Fe(CN)_6]_{0.98}\cdot 0.3H_2O$ (**1**), $Rb_{0.85}Mn[Fe(CN)_6]_{0.95}\cdot 0.8H_2O$ (**2**), and $Rb_{0.73}Mn[Fe(CN)_6]_{0.91}\cdot 1.4H_2O$ (**3**). Anal. Calcd for **1**: Rb, 23.1; Mn, 15.8; Fe, 15.7; C, 20.3; N, 23.6. Found: Rb, 22.9; Mn, 15.9; Fe, 15.7; C, 20.0; N, 23.5. Anal. Calcd for **2**: Rb, 21.2; Mn, 16.0; Fe, 15.5; C, 19.9; N, 23.3. Found: Rb, 21.3; Mn, 16.1; Fe, 15.2; C, 19.7; N, 23.5. Anal. Calcd for **3**: Rb, 18.6; Mn, 16.4; Fe, 15.2; C, 19.6; N, 22.8. Found: Rb, 18.5; Mn, 16.6; Fe, 15.2; C, 19.3; N, 23.1. The schematic structure of $Rb_xMn[Fe(CN)_6]_{(x+2)/3}\cdot zH_2O$ is shown in Figure 1. The SEM images demonstrated that the shapes for compounds **1**−**3** were rectangular and their sizes were 1.2 ± 0.6 (**1**), 1.0 ± 0.5 (**2**), and 1.1 ± 0.9 (**3**) μm.

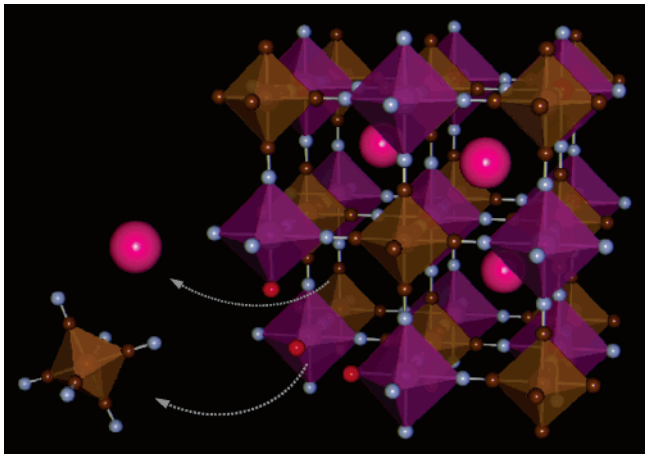

Figure 1. Schematic structure of $Rb_xMn[Fe(CN)_6]_{(x+2)/3}\cdot zH_2O$. Brown and purple polyhedrons describe [FeC_6] and [MnN_6 (or MnN_5O)], respectively. Large pink circles are Rb^I ions. Small brown circles are C atoms, small gray circles are N atoms, and small red circles are O atoms of ligand water. Zeolitic water molecules are omitted for clarity.

3.2. Bistability in Magnetic Susceptibility. Figure 2 shows the product of the molar magnetic susceptibility (χ_M) and the temperature (T) vs T plots for **1**−**3**. The χ_MT values for **1**−**3** at 300 K were 4.58, 4.50, and 4.45 cm^3 K mol^{-1}, respectively, which are consistent with their expected spin-only values of 4.74, 4.73, and 4.72 cm^3 K mol^{-1}, indicating that the electronic states of the HT phases are $Rb^I_{0.94}Mn^{II}[Fe^{III}(CN)_6]_{0.98}\cdot 0.3H_2O$ (**1**), $Rb^I_{0.85}Mn^{II}[Fe^{III}(CN)_6]_{0.95}\cdot 0.8H_2O$ (**2**), and $Rb^I_{0.73}Mn^{II}[Fe^{III}(CN)_6]_{0.91}\cdot 1.4H_2O$ (**3**). The χ_MT value of **1** decreased at 216 K ($T_{1/2\downarrow}$), as the sample was cooled at a cooling rate of −0.5 K min^{-1} (Figure 2a). Conversely, as the sample in the LT phase was warmed (heating rate +0.5 K min^{-1}), the χ_MT value increased around 302 K ($T_{1/2\uparrow}$) and reached the HT phase value. The transition temperature T_p ($= (T_{1/2\downarrow} + T_{1/2\uparrow})/2$) was 259 K, and the width of the thermal hysteresis loop ΔT ($= T_{1/2\uparrow} - T_{1/2\downarrow}$) was 86 K. The χ_MT-T plots for **2** showed $T_{1/2\downarrow} = 189$ K, $T_{1/2\uparrow} = 283$ K, $T_p = 236$ K, and $\Delta T = 94$ K (Figure 2b). The χ_MT-T plots for **3** showed $T_{1/2\downarrow} = 147$K, $T_{1/2\uparrow} = 263$ K, $T_p = 205$ K, and $\Delta T = 116$ K (Figure 2c). In this series, the T_p and ΔT values systematically changed depending on the Fe/Mn ratio of ($x + 2$)/3; i.e., the T_p value decreased and the ΔT value increased as the Fe/Mn ratio decreased. It is noteworthy that a surprisingly large ΔT value of 116 K is recorded for **3**.

3.3. Valence States of LT Phases. Figure 3a shows the CN^- stretching frequencies in the IR spectra for **1** at 300 and 100 K. At 300 K, a sharp CN^- peak was observed at 2152 cm^{-1}. As the temperature decreased, the intensity of this peak decreased and a new broad peak appeared around 2095 cm^{-1} at 100 K. The CN^- stretching peak at 2152 cm^{-1} in the HT phase is assigned to the CN^- ligand bridged to Fe^{III} and Mn^{II} ions ($Fe^{III}-CN^--Mn^{II}$), and the broad CN^- stretching peak at 2095 cm^{-1} in the LT phase is assigned to the CN^- ligand bridged to Fe^{II} and Mn^{III} ions ($Fe^{II}-CN^--Mn^{III}$). Similar temperature-induced changes in the IR spectra were observed in **2** and **3** as shown in parts b and c of Figure 3, respectively. By reference to the ratio between the IR intensities of $Fe^{III}-CN^--Mn^{II}$ and $Fe^{II}-CN^--Mn^{III}$ for

(10) (a) Ohkoshi, S.; Tokoro, H.; Utsunomiya, M.; Mizuno, M.; Abe, M.; Hashimoto, K. *J. Phys. Chem. B* **2002**, *106*, 2423. (b) Osawa, H.; Iwazumi, T.; Tokoro, H.; Ohkoshi, S.; Hashimoto, K.; Shoji, H.; Hirai, E.; Nakamura, T.; Nanao, S.; Isozumi, Y. *Solid State Commun.* **2003**, *125*, 237. (c) Moritomo, Y.; Kato, K.; Kuriki, A.; Taketa, M.; Sakata, M.; Tokoro, H.; Ohkoshi, S.; Hashimoto, K. *J. Phys. Soc. Jpn.* **2002**, *71*, 2078. (d) Tokoro, H.; Ohkoshi, S.; Matsuda, T.; Hashimoto, K. *Inorg. Chem.* **2004**, *43*, 5231.

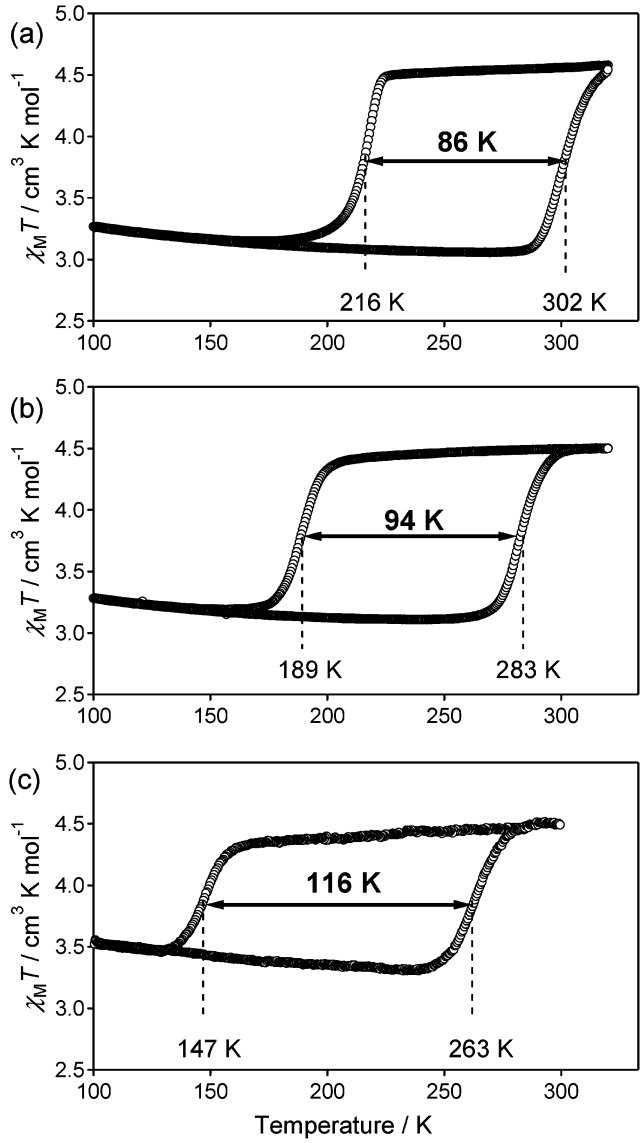

Figure 2. Observed $\chi_M T-T$ plots for **1** (a), **2** (b), and **3** (c).

RbMn[Fe(CN)$_6$],[10] the valence states of LT phases for **1**−**3**, $Rb^{I}_{x}Mn^{II}_{1-a}Mn^{III}_{a}[Fe^{II}(CN)]_a[Fe^{III}(CN)]_{((x+2)/3-a)}$ ($a = Mn^{III}/(Mn^{II} + Mn^{III})$), were evaluated.[11] As a result, a values were estimated to be 0.98 (**1**), 0.87 (**2**), and 0.65 (**3**), and the valence states of LT phases of **1**−**3** were assigned to $Rb^{I}_{0.94}Mn^{II}_{0.02}Mn^{III}_{0.98}[Fe^{II}(CN)_6]_{0.98}\cdot 0.3H_2O$, $Rb^{I}_{0.85}Mn^{II}_{0.13}Mn^{III}_{0.87}[Fe^{II}(CN)]_{0.87}[Fe^{III}(CN)]_{0.08}\cdot 0.8H_2O$, and $Rb^{I}_{0.73}Mn^{II}_{0.35}Mn^{III}_{0.65}[Fe^{II}(CN)]_{0.65}[Fe^{III}(CN)]_{0.26}\cdot 1.4H_2O$, respectively. The decrease of the conversion from Mn^{II} to Mn^{III} is explained by the coordinating environment of Mn sites. In $Rb_xMn[Fe(CN)_6]_{(x+2)/3}\cdot zH_2O$, the statistical probabilities of MnO_nN_{6-n} ($n = 0-5$) are expressed as the product of the combination ($_6C_n$) and existing probabilities of $(1 - x)/3$ for O atoms and $(x + 2)/3$ for N atoms, i.e., $_6C_n$ $((1 - x)/3)^n((x + 2)/3)^{6-n}$ and the statistical probabilities of the MnN_6 site for **1**−**3** are 0.89, 0.74, and 0.57, respectively. These probabilities roughly correspond to the observed $Mn^{III}/(Mn^{II} + Mn^{III})$ ratio, and hence, the conversion from Mn^{II} to Mn^{III} of this system is considered to depend on the number of MnN_6 sites which can undergo a Jahn−Teller distortion.

(11) Valence states were evaluated through the relationship of $a = [((Abs2)-(Abs3)((x + 2)/3))/((Abs1)(Abs4))]^{1/2}$, where Abs1 and Abs2 are CN peak intensities of $Fe^{III}-CN-Mn^{II}$ and $Fe^{II}-CN-Mn^{III}$, respectively, in target compounds (**1**, **2**, or **3**), and Abs3 and Abs4 are CN peak intensities of $Fe^{III}-CN-Mn^{II}$ and $Fe^{II}-CN-Mn^{III}$ in RbMn[Fe(CN)$_6$], respectively.

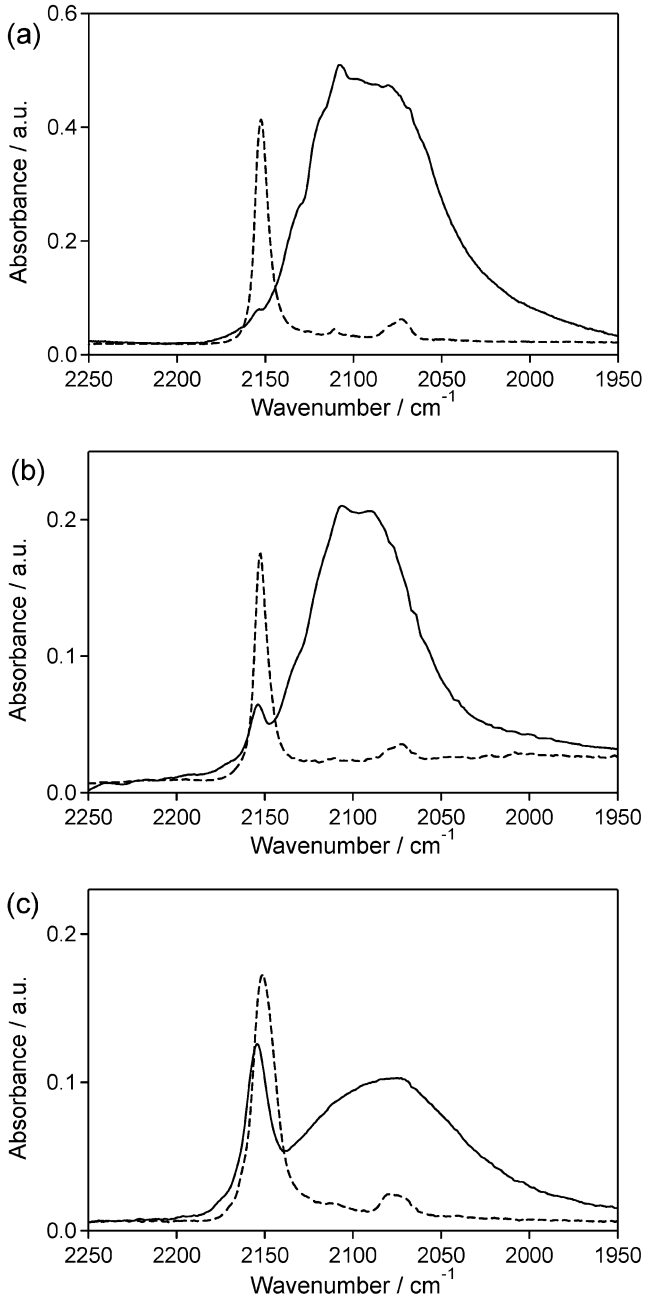

Figure 3. IR spectra for **1** (a), **2** (b), and **3** (c) at 300 (dotted line) and 100 (solid line) K.

3.4. Crystal Structures. The X-ray powder diffraction (XRD) pattern collected at 300 K showed that all of the HT phases were face-centered cubic ($F\bar{4}3m$). The lattice constants for **1**−**3** were $a = 10.561(1)$, 10.552(6), and 10.534(7) Å, respectively, as shown in the upper patterns of Figure 4. As the samples were cooled, the XRD peaks from the HT phase disappeared around $T_{1/2}$↓ and different patterns of XRD peaks appeared as shown in the lower patterns of Figure 4. The LT phases for **1** and **2** were tetragonal crystal structures ($I\bar{4}m2$) with lattice constants of $a = b = 7.087(1)$ Å and $c = 10.542(3)$ Å (**1**) and $a = b = 7.085(3)$ Å and $c = 10.503(5)$ Å (**2**). This transformation from cubic to tetragonal is also observed in RbMn[Fe(CN)$_6$], and the driving force

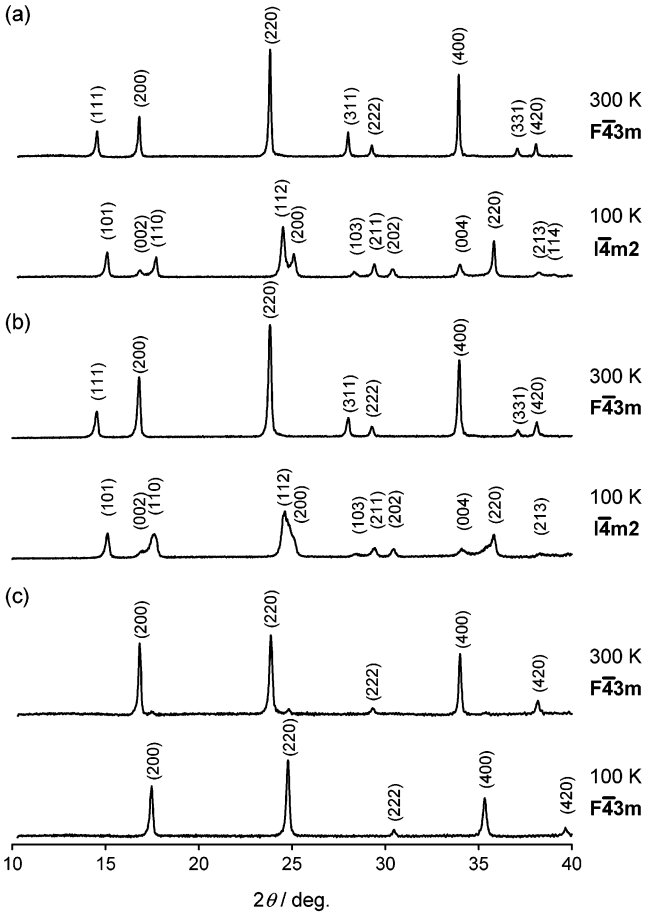

Figure 4. XRD patterns for **1** (a), **2** (b), and **3** (c) at 300 and 100 K.

of this structural distortion is ascribed to the Jahn−Teller effect on the Mn^{III} sites.[10] In contrast, the LT phase for **3** was not tetragonal, but had a cubic structure ($F\bar{4}3m$) with $a = 10.159(2)$ Å. Since the LT phase of **3** has a low $Mn^{III}/(Mn^{II} + Mn^{III})$ ratio of 0.65, the Jahn−Teller elongation of Mn^{III} may not occur in only one direction of the lattice, and thus, the LT phase of **3** exhibits a different structure.

3.5. Mechanism of the T_p Shift and ΔT Expansion. The systematic changes of T_p and ΔT values depend on the Fe/Mn ratio. Since the free energies (G_i) of the LT phase and HT phase depend on the enthalpy (H_i), entropy (S_i), and temperature, i.e., $G_i = H_i - S_iT$ (i = LT, HT), the T_p value is expressed by $T_p = \Delta H/\Delta S$, where ΔH ($= H_{HT} - H_{LT}$) is the transition enthalpy and ΔS ($= S_{HT} - S_{LT}$) is the transition entropy. This relationship suggests that the decrease of T_p is due to the decrease in $\Delta H/\Delta S$. In our compounds, the experimental T_p value decreases as the Fe/Mn ratio decreases. The mechanism of this is that the decrease of the conversion from Mn^{II} to Mn^{III} reduces the ΔH value and then the T_p value shifts to a low temperature via the decrease of $\Delta H/\Delta S$. In addition, the decrease in ΔH can also explain the expansion of the ΔT value in the thermal hysteresis loop. On the basis of the mean-field model proposed by Slichter et al.,[12] the free energy as a function of the HT phase fraction (α) and that of the LT phase fraction ($1 - \alpha$) is described by $G = \alpha\Delta H + \gamma\alpha(1 - \alpha) + T\{R[\alpha \ln \alpha + (1 - \alpha) \ln(1 - \alpha)] - \alpha\Delta S\}$. In this model, the temperature dependence

(12) Slichter, C. P.; Drickamer, H. G. *J. Chem. Phys.* **1972**, *56*, 2142.

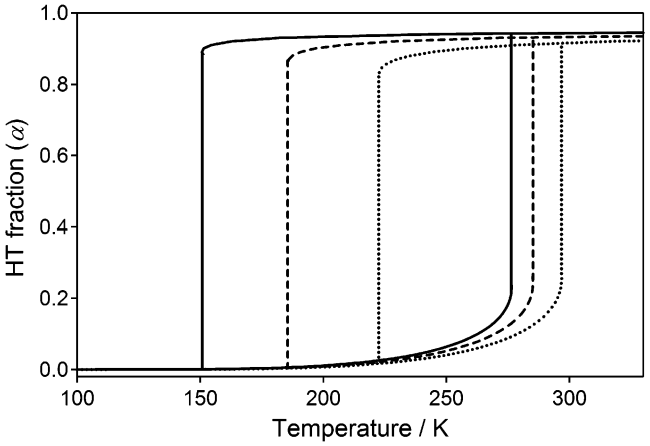

Figure 5. Calculated temperature-induced phase transition with hysteresis loops using the mean-field model proposed by Slichter and Drickamer:[12] HT phase fraction (α) vs temperature plots for $\Delta H = 6.9$ (dotted line), 6.5 (dashed line), and 6.2 (solid line) kJ mol^{-1} at $\gamma = 6.5$ kJ mol^{-1} and $\Delta S = 25$ J K^{-1} mol^{-1}.

of α is given by $\ln((1 - \alpha)/\alpha) = (\Delta H + \gamma(1 - 2\alpha))/RT - \Delta S/R$, where R is the gas constant and γ is an interaction parameter. Figure 5 shows the α vs temperature plots for $\Delta H = 6.9$, 6.5, and 6.2 kJ mol^{-1} when a cooperative force and ΔS value of the system are set to constant values of $\gamma = 6.5$ kJ mol^{-1} and $\Delta S = 25$ J K^{-1} mol^{-1}. The model calculation suggests that the ΔT value increases as ΔH decreases. Hence, the decrease in ΔH due to the low conversion from Mn^{II} to Mn^{III} explains the observed trends of the decrease in T_p and the expansion of ΔT for this series.

4. Conclusion

A material that exhibits a thermal phase transition with a thermal hysteresis loop is useful for an application such as in memory devices. In this paper, we report that a series of $Rb_xMn[Fe(CN)_6]_{(x+2)/3}\cdot zH_2O$ compounds exhibit a temperature-induced phase transition with a surprisingly large thermal hysteresis loop that depends on x, i.e., 86 K ($x = 0.94$), 94 K ($x = 0.85$), and 116 K ($x = 0.73$). The observed thermal hysteresis of 116 K is the second largest value observed for a reversible thermal hysteresis loop[13] and the largest value for a phase transition in an Fe-based compound. The origin of a thermal hysteresis loop is a strong cooperativity in 3-D structure. Since new building blocks for cyano-bridged metal complex assemblies are currently being prepared,[14] various phase transition phenomena with a thermal hysteresis loop will be observed with cyano-bridged metal complex assemblies soon.

Acknowledgment. We thank Mr. T. Hozumi for preparing the color illustration. The present research is supported in part by a grant for the 21st Century COE Program "Human-Friendly Materials based on Chemistry" and a Grand-in-Aid for Scientific Research from the Ministry of Education, Culture, Sports, Science, and Technology of Japan.

CM048461X

(13) Jung, O. S.; Jo, D. H.; Lee, Y. A.; Conklin, B. J.; Pierpont, C. G. *Inorg. Chem.* **1997**, *36*, 19.

(14) (a) Beauvais, L. G.; Long, J. R. *J. Am. Chem. Soc*. **2002**, *124*, 2110. (b) Lescouëzec, R.; Vaissermann, J.; Lloret, F.; Julve, M.; Verdaguer, M. *Inorg. Chem.* **2002**, *41*, 5943. (c) Bennett, M. V.; Long, J. R. *J. Am. Chem. Soc.* **2003**, *125*, 2394. (d) Smith, J. A.; Galán-Mascarós, J. R.; Clérac, R.; Sun, J. S.; Ouyang, X.; Dunbar, K. R. *Polyhedron* **2001**, *20*, 1727.